ACS Combinatorial Science



Article

# Benzimidazolyl-pyrazolo[3,4-b]pyridinones - selective inhibitors of MOLT-4 leukemia cell growth and sea urchin embryo spiculogenesis: Target quest.

Boris V. Lichitsky, Andrey N. Komogortsev, Arkady A. Dudinov, Mikhail M Krayushkin, Evgenii N. Khodot, Alexander V. Samet, Eugenia Silyanova, Leonid D. Konyushkin, Alexei S Karpov, Delphine Gorses, Thomas Radimerski, Marina N. Semenova, Alex S. Kiselyov, and Victor Vladimirovich Semenov

*ACS Comb. Sci.*, **Just Accepted Manuscript** • DOI: 10.1021/acscombsci.9b00135 • Publication Date (Web): 05 Nov 2019



## Just Accepted



is published by the American Chemical Society. 1155 Sixteenth Street N.W., Washington, DC 20036

# Benzimidazolyl-pyrazolo[3,4-*b*]pyridinones - selective inhibitors of MOLT-4 leukemia cell growth and sea urchin embryo spiculogenesis: Target quest

Boris V. Lichitsky,[†] Andrey N. Komogortsev,[†] Arkady A. Dudinov,[†] Mikhail M. Krayushkin,[†] Evgenii N. Khodot,[†] Alexander V. Samet,[†] Eugenia A. Silyanova,[†] Leonid D. Konyushkin,[†] Alexei S. Karpov,[‡] Delphine Gorses,[‡] Thomas Radimerski,[‡] Marina N. Semenova,[§] Alex S. Kiselyov,[‖] Victor V. Semenov*,[†]

[†] N. D. Zelinsky Institute of Organic Chemistry, RAS, Leninsky Prospect, 47, 119991, Moscow, Russian Federation

[‡] Novartis Institutes for BioMedical Research, CH-4056 Basel, Switzerland

[§] N. K. Kol'tsov Institute of Developmental Biology, RAS, Vavilov Street, 26, 119334, Moscow, Russian Federation

[‖] Myocea, Inc., 9833 Pacific Heights Blvd., San Diego, CA 92121, USA

Corresponding author: Victor V. Semenov

Address: N. D. Zelinsky Institute of Organic Chemistry, RAS, Leninsky Prospect, 47, 119991, Moscow, Russian Federation. Tel.: +7 499 135 6343; fax: +7 499 137 2966.

E-mail: vs@zelinsky.ru

## ABSTRACT

1,3-Substituted pyrazolo[3,4-*b*]pyridinones **11**–**18** were synthesized by a three-component condensation of Meldrum's acid with aryl aldehydes and 1,3-substituted 5-aminopyrazoles. Their biological activity was evaluated using the *in vivo* phenotypic sea urchin embryo assay and the *in vitro* cytotoxicity screen against human cancer cell lines. In the sea urchin embryo model, 1-benzimidazolyl-pyrazolo[3,4-*b*]pyridinones **11** caused inhibition of hatching and spiculogenesis at submicromolar concentrations. These compounds also selectively and potently inhibited growth of the MOLT-4 leukemia cell line. Subsequent structure-activity relationship studies determined the benzimidazolyl fragment as an essential pharmacophore for both effects. We applied numerous techniques for the target identification. A preliminary QSAR target identification search did not result in tangible leads. Attempts to prepare a relevant photoaffinity probe that retained potency in both assays were not successful. Compounds **11** were further characterized for their activity in ~~a~~ wild type *vs* Notch-mutant leukemia cell lines, and in *in vitro* panels of kinases and matrix metalloproteinases. Using a series of diverse modulators of spiculogenesis as standards, we excluded multiple signaling networks including Notch, Wnt/β-catenin, receptor tyrosine kinases (VEGF/VEGFR, FGF/FGFR), PI3K, and Raf-MEK-ERK as possible targets of **11**. On the other hand, matrix metalloproteinase-9/hatching enzyme was identified as one potential target.


**KEYWORDS:** *benzimidazolyl-pyrazolo[3,4-b]pyridinone, cytotoxicity, MOLT-4, sea urchin embryo, spiculogenesis*

## INTRODUCTION

Multicomponent domino reactions are versatile tools for expeditious access to a variety of biologically active compounds. For instance, a three-component condensation of Meldrum's acid **1** with aromatic aldehydes **2** and 5-membered aminoheterocycles **A** (amino-imidazoles, -pyrazoles, -thiazoles, isothiazoles, thiophenes) furnishes diverse dihydropyridones **B** (Figure 1).[1] In a further development of this protocol, we introduced a facile synthesis of 3,7-diaryl-6,7-dihydroisothiazolo-[4,5-b]pyridin-5(4*H*)-ones **C**. Gratifyingly, multiple derivatives from these series including compound **C1** (Figure 1) were identified to be potent antimitotics with microtubule destabilizing mode of action, as demonstrated by the *in vivo* phenotypic sea urchin embryo model.[2] Furthermore, selected compounds displayed a significant cytotoxicity against human cancer cells including multidrug resistant cell lines with $GI_{50}$ values less than 1 μM.[2]

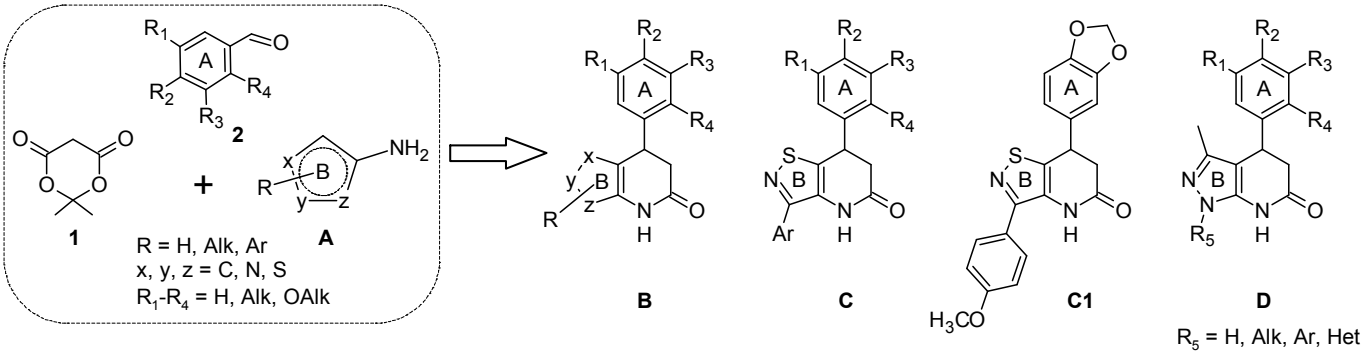


**Figure 1.** Reaction scheme for azolopyridinones.

In the ongoing search for the novel tubulin destabilizing agents, we turned our attention to a chemotype **B**, and the respective pyrazolo[3,4-b]pyridinones **D** in particular. The synthesis of pyrazolopyridinone derivatives **D** has been explored recently.[3-7] Roshan, *et al.* reported a one-pot, three-component reaction to access novel derivatives of pyrazolo[3,4-*b*]pyridine-6(7*H*)-ones (Figure 1, **D**, $R_5$ = H,) with excellent yields (87%–95%) from 5-amino-3-methyl-1*H*-pyrazole.[3] Several analogues exhibiting general structure **D** displayed a diverse spectrum of biological activities including antimicrobial,[4, 8] antiviral,[9] anti-inflammatory,[10] GSK3-inhibiting,[11] and proapoptotic[8] effects. In a recent publication, these molecules were identified as agonists of the G-protein coupled receptor 39 (GPR39).[12]

Encouraged by these data, we synthesized a series of compounds represented by the general scaffold **D** with diverse substituents $R_1$–$R_4$ in the aromatic ring A and $R_5$ in the pyrazole ring B. Biological activities, structure-activity relationship (SAR), and possible mechanism(s) of action of these targeted compounds were evaluated using a phenotypic sea urchin embryo model, human cancer cell lines, and biochemical target-based screen.

## RESULTS AND DISCUSSION

**Chemistry.** 1,3-Substituted pyrazolo[3,4-*b*]pyridine-6(7*H*)-ones **11**–**18** were synthesized using three-component condensation of Meldrum's acid **1**, aryl aldehydes **2**, and 1,3-substituted 5-aminopyrazoles **3**–**10** (Scheme 1).

**Scheme 1.** Synthesis of pyrazolo[3,4-*b*]pyridinones **11**–**18**.

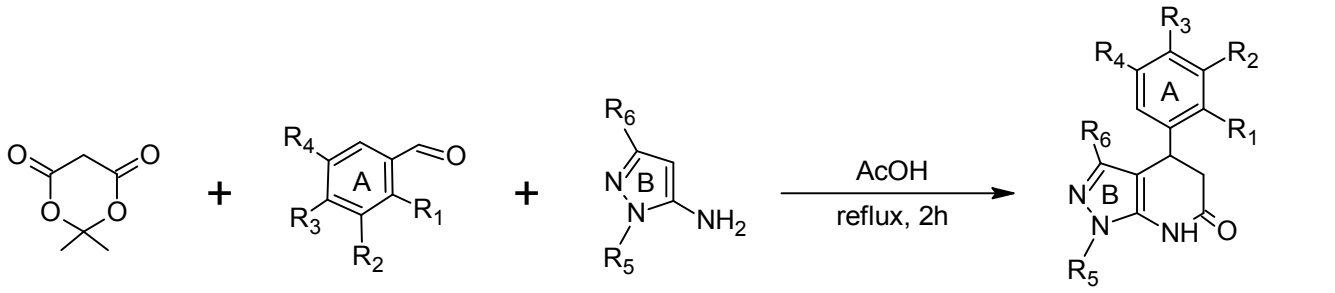


**1** **2a-v** **3-10** **11a-u; 12j; 13b,j; 14d,f,g; 15b,j; 16c,j,o; 17v; 18b,j**

| | $R_1$ | $R_2$, | $R_3$ | $R_4$ |
|---|---|---|---|---|
| **a:** | H | H | OH | H |
| **b:** | H | H | OMe | H |
| **c:** | H | OMe | H | H |
| **d:** | H | OMe | OH | H |
| **e:** | H | OH | OMe | H |
| **f:** | H | OMe | OMe | H |
| **g:** | H | $-OCH_2O-$ | | H |
| **h:** | H | OMe | H | OMe |
| **i:** | OMe | OMe | H | H |
| **j:** | H | OMe | OH | OMe |
| **k:** | H | OMe | OMe | OMe |
| **l:** | H | OMe | $-OCH_2O-$ | |
| **m:** | OMe | OMe | OMe | OMe |
| **n:** | OMe | $-OCH_2O-$ | | OMe |
| **o:** | OMe | OMe | $-OCH_2O-$ | |
| **p:** | H | OMe | $OCH_2CONH_2$ | H |
| **q:** | H | H | $OCH_2$-4F-$C_6H_4$ | H |
| **r:** | H | H | $OCH_2$-2Cl-$C_6H_4$ | H |
| **s:** | 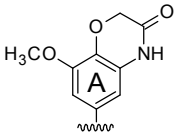 | | | |
| **t:** | H | OMe | $OC_7H_{15}$ | OMe |
| **u:** | H | OMe | $OC_9H_{19}$ | OMe |
| **v:** | H | OMe | OEt | H |

| Cmpd | $R_5$ | $R_6$ |
|---|---|---|
| **3, 11:** | 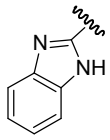 | Me |
| **4, 12:** | Me | Me |
| **5, 13:** | Me | H |
| **6, 14:** | 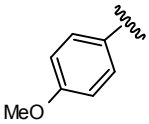 | Me |
| **7, 15:** | 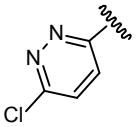 | Me |
| **8, 16:** | 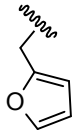 | H |
| **9, 17:** | 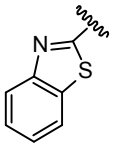 | H |
| **10, 18:** | H | H |

In the modified procedure to make benzimidazolyl-pyrazolo[3,4-*b*]pyridinones (BIPP) **11a**–**u**, we improved both feasibility and yield of the key intermediate, 2-hydrazinyl-1*H*-benzimidazole **21** (Scheme 2, A). Specifically, starting benzimidazole-2-thione **19** was oxidized easily with aqueous sodium percarbonate to afford 1*H*-benzimidazole-2-sulfonic acid **20**. Further conversion of **20** into **21** was accomplished in the aqueous $N_2H_4$ at moderate pressure under heating. Compound **21** was further reacted with cyanoacetone to afford the intermediate 1-(1*H*-benzimidazol-2-yl)-3-methyl-1*H*-pyrazol-5-amine **3** followed by its three-component condensation to furnish the desired derivatives **11a**–**u** (Scheme 2, B, 49–82% overall yields). Further modifications of the benzimidazole

pharmacophore were accomplished *via* base-mediated alkylation of the NH to result in **11bx**, **11by**, **11jx**, **11jy**, and **11jz**.

**Scheme 2.** Synthesis of benzimidazolyl-pyrazolo[3,4-*b*]pyridinones **11** (BIPP).

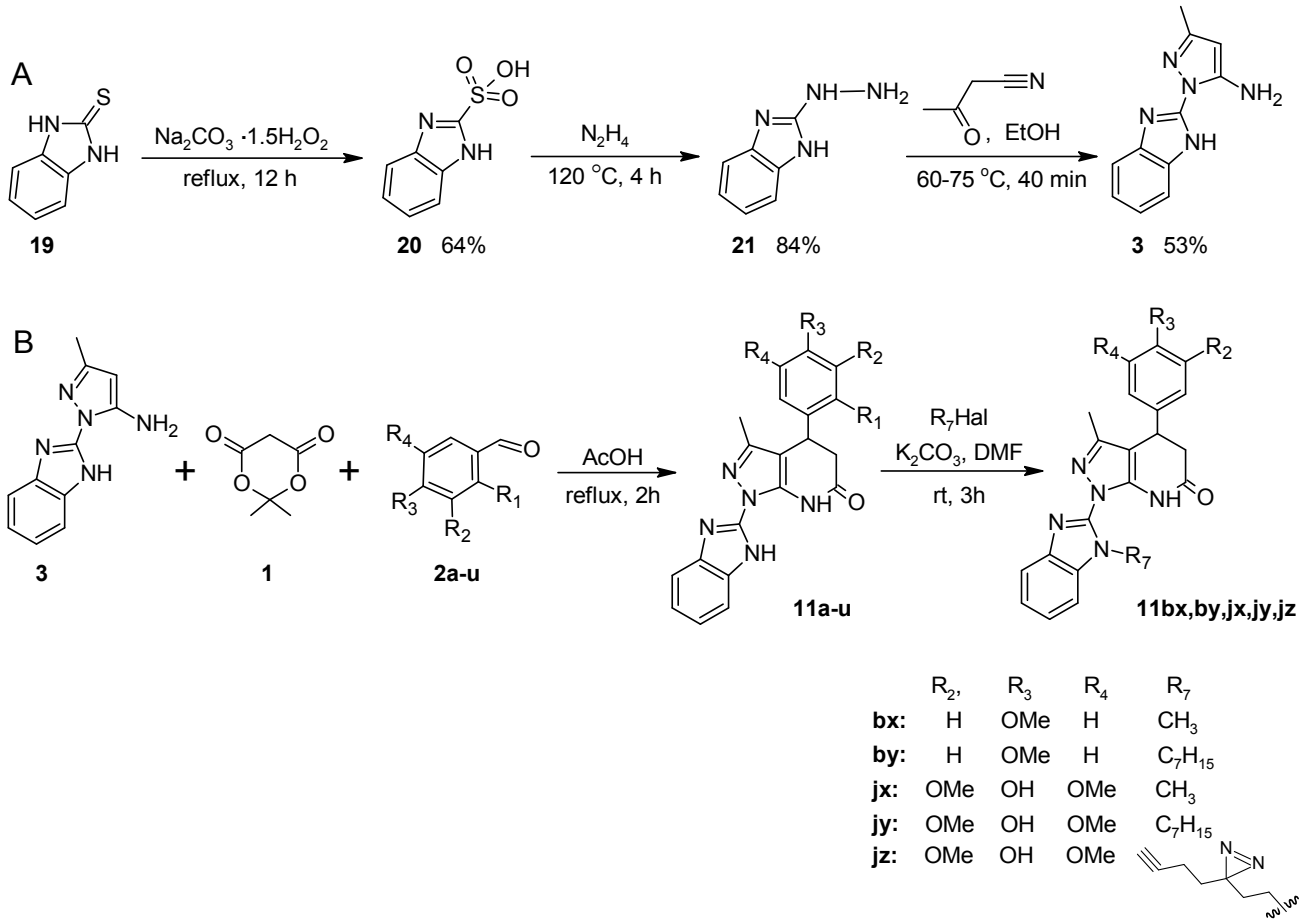


**Phenotypic Sea Urchin Embryo Tests.** Considering the reported antimitotic microtubule destabilizing activity of isothiazolopyridinones **C** (Figure 1),[2] we decided to evaluate related pyrazolopyridinones **11**–**18** for their antitubulin activity using a phenotypic sea urchin embryo assay. The assay was developed and extensively validated by our group over the past decade. It provides data on the specific antimitotic microtubule destabilizing activity related to several particular steps of differentiation and morphogenesis of the embryo.[13, 14] Particularly, cleavage (cell division) alteration/arrest after fertilized egg treatment evidences antimitotics activity. Specific changes of embryo motility after treatment of hatched blastulae including spinning at the bottom of the vessel instead of forward swimming near the seawater surface evidences microtubule destabilizing mode of action. The effects of compounds **11**–**18** on the sea urchin embryos are summarized in Tables 1 and 2. A close analogue of **14g**, isothiazolopyridinone **C1** (Figure 1),[2] and natural antimitotic

combretastatin A4 disodium phosphate (CA4P) served as reference compounds. In contrast to isothiazolopyridinones,[2] only four molecules were characterized as antimitotic antitubulin agents. Specifically, pyrazolopyridinones **14g** and **16o** induced cleavage alteration/arrest and embryo spinning, whereas **14d** and **17v** triggered the formation of tuberculate-shaped arrested eggs, both effects are suggestive of the microtubule destabilizing activity. Notably, pyrazolopyridinone **14g** was less active than its isothiazole analog **C1**. The majority of pyrazolopyridinones caused neither cleavage arrest with tuberculate eggs, nor embryo spinning, the phenotypic effects directly linked to microtubule destabilization. Compounds **11e**, **11m**–**p**, **14f**, **15b**, **16c**, and **18b** exhibited modest antiproliferative activity altering cleavage at relatively high concentrations (1–4 μM). However, it should be pointed out that, as opposed to tubulin/microtubule targeting compounds, numerous benzimidazolyl-pyrazolopyridinones (BIPP) **11**, namely, **11a**–**q**, and **11s**, selectively inhibited spiculogenesis, a formation of the embryonic skeleton (Figure 2A), with good potency (EC values of 0.05–1 μM, Table 1). Most of these compounds, specifically, **11a**, **11e**–**j**, **11k**, **11l**, **11o**, **11p**, and **11s**, also inhibited hatching at concentrations of 0.5–4 μM, higher than those necessary for spicule impairments (Figure 2B). These two well-known phenotypic effects that are not exhibited by antitubulin agents were readily observed and are likely to be related to distinct developmental processes discussed below.

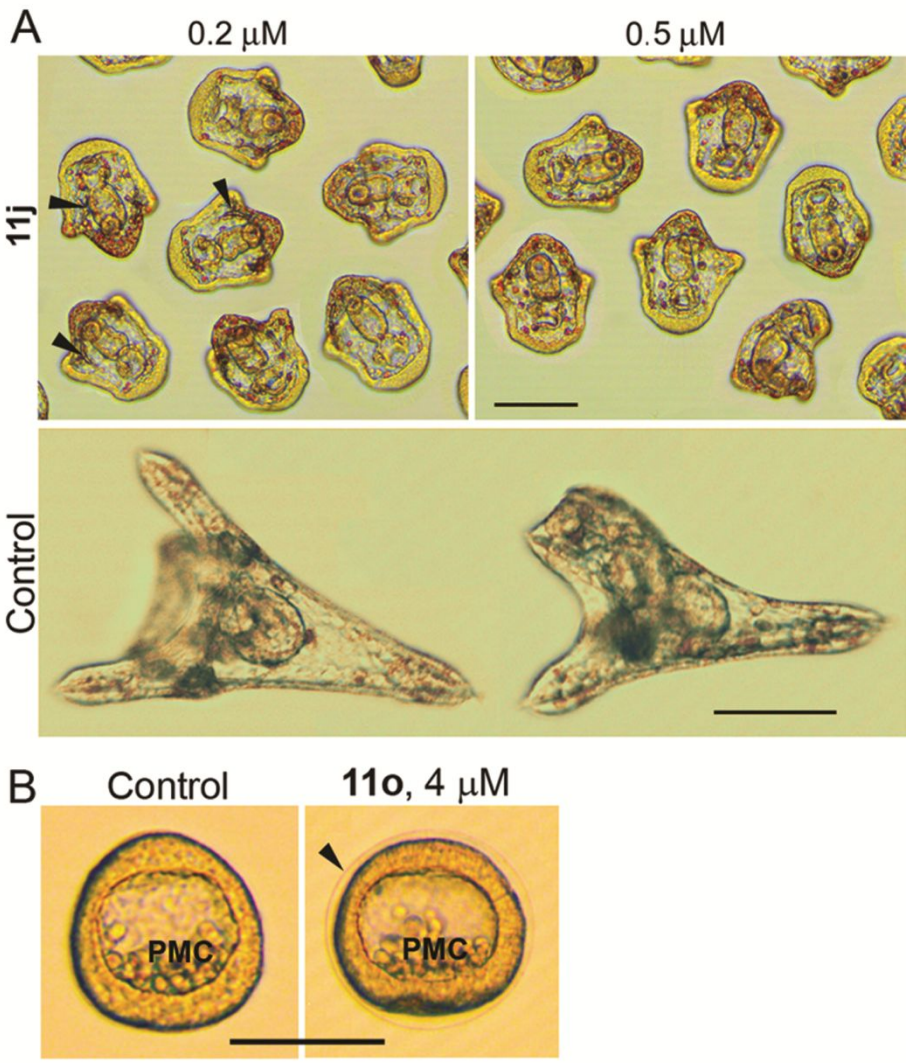


**Figure 2.** Typical effects of benzimidazolyl-pyrazolopyridinones (BIPP) **11** on the sea urchin embryos as exemplified by **11j** (A, 30 h postfertilization) and **11o** (B, 12 h postfertilization). Compounds were added to fertilized eggs. (A) **11j** (0.2 and 0.5 μM) selectively inhibited spiculogenesis. At 0.2 μM concentration spicule rudiments (arrowheads) are visible in some embryos. Control: Intact two-arm plutei. (B) Control: Intact hatched mesenchyme blastula with primary mesenchyme cells (PMC) inside blastocoel. **11o** (4 μM) caused hatching arrest, and mesenchyme blastula developed inside fertilization envelope (arrowhead). Incubation temperature: 24 °C. Scale bars: 100 μm.

**Table 1. Effects of Benzimidazolyl-pyrazolopyridinones 11 on MOLT-4 Cells and Sea Urchin Embryos**

| compd | sea urchin embryo effects, EC (μM)[a] | | | | NCI60 screen, SRB assay | | resazurin assay |
|---|---|---|---|---|---|---|---|
| | cleavage alteration | hatching inhibition | spicule alteration | no spicules | $GI_{50}$ (μM)[b], MOLT-4/mean for 60 cell lines | growth %[c], MOLT-4/mean for 60 cell lines | MOLT-4 $GI_{50}$ (μM)[b] (mean ± SE) |
| **11a** | >4 | 2 | 0.2 | 0.5 | NA[d] | -14.44/80.04 | 0.11 ± 0.01 |
| **11b** | >4 | >4 | 0.2 | >4 | 0.0657/2.69 | -44.57/77.08 | 0.17 ± 0.03 |
| **11c** | >4 | 4 | 2 | >4 | NA[d] | NA[d] | 0.21 ± 0.03 |
| **11d** | >4 | 1 | 0.05 | 0.2 | NA[d] | NA[d] | 0.11 ± 0.01 |
| **11e** | 4 | 0.5 | 0.05 | 0.2 | NA[d] | NA[d] | 0.08 ± 0.01 |
| **11f** | >4 | 4 | 0.2 | 0.5 | 0.0405/4.27 | -31.49/63.48 | 0.12 ± 0.01 |
| **11g** | >4 | 2 | 1 | 4 | 0.0367/2.34 | -48.45/28.61 | 0.20 ± 0.03 |
| **11h** | >4 | 2 | 0.1 | 2 | NA[d] | NA[d] | 0.20 ± 0.03 |
| **11i** | >4 | 4 | 1 | 4 | 0.0478/3.89 | -30.97/62.58 | 0.12 ± 0.01 |
| **11j** | >4 | 2 | 0.05 | 0.2 | 0.0427/2.75 | -36.03/44.18 | 0.16 ± 0.01 |
| **11k** | >4 | 4 | 0.2 | 0.5 | NA[d] | -42.49/96.79 | 0.26 ± 0.02 |
| **11l** | >4 | 1 | 0.1 | 4 | NA[d] | NA[d] | 0.12 ± 0.01 |
| **11m** | 1 | >0.5 | 0.1 | 2 | NA[d] | NA[d] | 0.23 ± 0.05 |
| **11n** | 1 | >0.5 | 0.1 | 2 | NA[d] | NA[d] | NA[d] |
| **11o** | 4 | 1 | 0.1 | 4 | NA[d] | NA[d] | NA[d] |
| **11p** | 4 | 2 | 0.1 | 0.5 | NA[d] | NA[d] | 0.12 ± 0.01 |
| **11q** | >4 | >4 | 0.1 | 1 | NA[d] | 7.48/60.01 | 4.1 ± 0.5 |
| **11r** | >4 | >4 | 4 | >4 | NA[d] | 57.24/84.68 | NA[d] |
| **11s** | >4 | 2 | 0.1 | 0.5 | NA[d] | NA[d] | NA[d] |
| **11t** | >4 | >4 | 2 | >4 | NA[d] | NA[d] | 6.4 ± 1.6 |

| | | | | | | | |
|---|---|---|---|---|---|---|---|
| **11u** | >4 | >4 | 4 | >4 | NA[d] | NA[d] | NA[d] |
| **11bx** | >4 | >4 | >4 | >4 | NA[d] | NA[d] | NA[d] |
| **11by** | >4 | >4 | >4 | >4 | NA[d] | NA[d] | NA[d] |
| **11jx** | >4 | >4 | >4 | >4 | NA[d] | NA[d] | 4.5 ± 0.9 |
| **11jy** | >4 | >4 | 4 | >4 | NA[d] | NA[d] | >10 |
| **11jz** | >4 | >4 | >4 | >4 | NA[d] | NA[d] | NA[d] |
| **C1**[2] | 0.01 | NA[d] | NA[d] | NA[d] | 1.29/1.55 | 81.63/77.34 | NA[d] |

[a] The sea urchin embryo assay was conducted as described previously.[13, 14] Fertilized eggs and hatched blastulae were exposed to 2-fold decreasing concentrations of compounds. Duplicate measurements showed no differences in effective threshold concentration (EC) values. No cleavage arrest and embryo spinning were observed. [b] $GI_{50}$: concentration required for 50% cell growth inhibition. [c] Cell growth at 10 $\mu$M concentration. [d] NA: not available.

**Table 2. Effects of Pyrazolo[3,4-*b*]pyridinones 12–18 on MOLT-4 Cells and Sea Urchin Embryos**

| compd | sea urchin embryo effects, EC (μM)[a] | | | | NCI60 screen, SRB assay | | resazurin assay |
|---|---|---|---|---|---|---|---|
| | cleavage alteration | cleavage arrest | embryo spinning | spicule alteration | $GI_{50}$ (μM)[b], MOLT-4/mean for 60 cell lines | growth %[c], MOLT-4/mean for 60 cell lines | MOLT-4 $GI_{50}$ (μM)[b] |
| **12j** | >4 | >4 | >4 | >4 | NA[d] | 103.38/96.99 | >10 |
| **13b** | >4 | >4 | >4 | >4 | NA[d] | NA[d] | NA[d] |
| **13j** | >4 | >4 | >4 | >4 | NA[d] | NA[d] | NA[d] |
| **14d** | 0.5 | 2 TE[e] | >10 | NA[d] | NA[d] | NA[d] | NA[d] |
| **14f** | 4 | >4 | >4 | >4 | NA[d] | NA[d] | NA[d] |
| **14g** | 0.05 | 0.5 | 2 | NA[d] | NA[d] | NA[d] | NA[d] |
| **15b** | 2 | >4 | >4 | >4 | NA[d] | NA[d] | NA[d] |
| **15j** | >4 | >4 | >4 | >4 | NA[d] | NA[d] | NA[d] |
| **16c** | 2 | >4 | >4 | >4 | NA[d] | 127.27/101.63 | NA[d] |

| | | | | | | | |
|---|---|---|---|---|---|---|---|
| **16j** | >4 | >4 | >4 | >4 | NA[d] | NA[d] | NA[d] |
| **16o** | 0.2 | 1 | 4 | NA[d] | 0.600/0.562 | 1.51/19.05 | NA[d] |
| **17v** | 0.5 | 1 TE[e] | >5 | NA[d] | NA[d] | NA[d] | NA[d] |
| **18b** | 4 | >4 | >4 | >4 | NA[d] | NA[d] | NA[d] |
| **18j** | >4 | >4 | >4 | >4 | NA[d] | 97.59/97.77 | NA[d] |
| **C1**[2] | 0.01 | 0.1 | 0.2 | NA[d] | 1.29/1.55 | 81.63/77.34 | NA[d] |
| CA4P[2] | 0.005 | 0.01 | 0.05 | NA[d] | 0.00025/0.00171[f] | NA[d] | NA[d] |

[a] The sea urchin embryo assay was conducted as described previously.[13, 14] Fertilized eggs and hatched blastulae were exposed to 2-fold decreasing concentrations of compounds. Duplicate measurements showed no differences in effective threshold concentration (EC) values. No hatching inhibition was observed. [b] $GI_{50}$: concentration required for 50% cell growth inhibition. [c] Cell growth at 10 $\mu$M concentration. [d] NA: not available. [e] TE: tuberculate eggs typical of microtubule destabilizing agents. [f] NCI60 screen data for NSC #645646, combretastatin A-4 disodium phosphate (CA4P).

The structure-activity relationship (SAR) analysis suggested the importance of the benzimidazole fragment for the observed specific sea urchin embryo effects. Namely, compounds **12**–**18** lacking benzimidazole moiety, **12j**, **13b**, **13j**, **14f**, **15b**, **15j**, **16c**, **16j**, **18b**, and **18j**, did not induce either specific inhibition of hatching or spicule formation (Tables 1 and 2). Interestingly, replacement of the benzimidazole group changed biological activity of the resulting derivatives in the sea urchin embryo assay. For example, molecules **14d**, **14g**, **16o**, and **17v** were identified as microtubule destabilizing agents. These data were in contrast to the outcome shown by respective benzimidazole-containing analogues **11d**, **11g**, **11o**, and **11f** that inhibited hatching and spiculogenesis. Substitution at the *N* atom of the benzamidazole fragment (**11bx**, **11by**, **11jx**, and **11jy**) caused activity loss, as compared to **11b** and **11j**. Alkylation of the 4-OH pharmacophore in the aromatic ring A also yielded inactive compounds **11t** and **11u**. We did not observe any SAR correlation between the rate of hatching delay/arrest and suppression of spicule formation, suggesting possible interaction of BIPP **11** with more than one cellular target.

**Cytotoxicity Against Human Cancer Cells.** Compounds **11a**, **11b**, **11f**, **11g**, **11i–k**, **11q**, **11r**, **12j**, **16c**, **16o**, and **18j** were tested in the NCI60 screen to assess cytotoxicity against 60 human cancer cell lines using sulforhodamine B (SRB) assay. The results are presented in Tables 1 and 2. Molecules **11b**, **11f**, **11g**, **11i**, and **11j** containing substituted benzimidazole fragment were tested at five doses. Interestingly, they were found to selectively and potently inhibit growth of MOLT-4 human T-cell acute lymphoblastic leukemia cells with $GI_{50} < 0.1$ μM (Table 1, Supplementary Figures S1–S10). Notably, the compounds modulated growth of MOLT-4 cells in a dose dependent fashion with growth inhibition reaching maximum at 1 μM concentration. This MOLT-4 specificity was not observed at a higher concentrations (10–100 μM) as demonstrated in Supplementary Figures S1, S3, S5, S7, S9, and S11–S15, with the exception of **11k** that exhibited selectivity against MOLT-4 cells at 10 μM concentration (Table 1, Supplementary Figure S16). BIPP **11a**, **11q**, and **11r** tested at 10 μM concentrations also didn't display selectivity against MOLT-4 cells (Supplementary Figures S17–S19). Replacement of benzimidazole in **11j** with methyl group yielded inactive compound **12j** (Table 2). Similarly, related derivatives featuring (furan-2-yl)methylimidazole ring B showed neither cytotoxicity at up to 10 μM concentration (**16c**), nor selectivity against MOLT-4 cells (**16o**, Table 2, Supplementary Figures S20 and S21). Compound **18j** with unsubstituted imidazole ring B was inactive as well (Table 2).

In the next step, we tested a set of BIPP (**11a**–**m**, **11p**, **11q** and **11t**) and compound **12j** for MOLT-4 cell viability/proliferation using resazurin assay selected due to its validation, reliability and high dynamic range.[15, 16] In this test system, molecules **11** containing the benzimidazole fragment displayed high activity with $GI_{50}$ values of 0.077–0.257 μM (Table 1) except for **11q** and **11t** with bulky substituents in the aromatic ring A ($GI_{50} = 4.1 \pm 0.5$ and $6.4 \pm 1.6$ μM, respectively). **12j** lacking the benzimidazole fragment was inactive.

Thus far, cytotoxicity SAR studies revealed that the benzimidazole pharmacophore attached to the pyrazolopyridinone template as well as the hydroxy- and/or methoxy-substituted phenyl ring A were both essential for the selective MOLT-4 cells growth inhibition. Neither the number of hydroxy/methoxy substitutients nor their position in the phenyl ring A influenced this activity. On the contrary, introduction of bulky substituents into the ring A (compounds **11q**, **11r**, and **11t**) decreased the respective cytotoxicity.

Importantly, SAR analysis showed good correlation between selective cytotoxicity against MOLT-4 cells and phenotypic sea urchin embryo data. Potent and selective inhibitors of MOLT-4 cell growth, BIPP **11a**–**m** and **11p** also caused hatching inhibition and specifically altered spiculogenesis in sea urchin embryos (Table 1). Compounds lacking benzimidazole moiety, **12j**, **16c**, and **18j** were not selective against MOLT-4 cells. These molecules did not induce specific inhibition of hatching or spicule formation (Table 2). A weak cytotoxic agent **11r** modestly modulated spicule growth in the sea urchin embryo. It is likely that the replacement of the benzimidazole group affected biological activity of the resulting derivatives in both assays. For example, molecule **16o** induced cleavage alteration/arrest and the embryo spinning, both suggestive of its microtubule destabilizing activity. In the NCI60 screen, this compound showed cytotoxicity (mean $GI_{50}$ = 0.562 μM) without specific inhibition of MOLT-4 cell growth typical for tubulin/microtubule targeting agents (for example, see NCI cancer screen data for combretastatin A-4, NSC # 613729, https://dtp.cancer.gov/dtpstandard/cancerscreeningdata/index.jsp). Our SAR data suggested that specific inhibition of both MOLT-4 cell growth and the sea urchin embryo spiculogenesis caused by BIPP **11** may be mediated by the same set of molecular targets or their sea urchin orthologues. Furthermore, *in vivo* sea urchin embryo assay data led us to conclude that cancer cell growth inhibition caused by BIPP **11** was not related to the microtubule destabilizing activity. Thus, in the next step we attempted to study possible cell target(s) and mechanism of action for the lead series **11**.

**Search for a Possible Cellular Target of BIPP 11.** In the initial approach, we analyzed the ChEMBL bioactivity database in order to identify related structures and link them to a specific molecular target(s). Unfortunately, the query yielded a single match, namely the compound **11a**. Whereas the molecule showed activity against parasitic protozoans (kinetoplastids), its $IC_{50}$ values against THP-1 human monocytic leukemia cells and HepG2 human liver carcinoma cells were 6.31 and 25.12 μM, respectively (http://dx.doi.org/10.6019/CHEMBL3430912). Neither mode of action nor cellular target data were available from the literature.

Considering that MOLT-4 is a Notch mutant cell line, we next conducted cytotoxicity studies of compound **11j** on 7 wild type (wt) and 4 Notch-mutant leukemia cell lines (Table 3). The tests showed no preferential inhibition of Notch mutants compared to MOLT-4 cell line. Specifically, three Notch-mutant leukemia cell lines as well as all wt lines were much less sensitive towards **11j**. Compound **12j** featuring methyl group instead of benzimidazole functionality was inactive. These results correlated well with the respective NCI60 screen data (Table 3) suggesting that the series of interest do not affect Notch signaling.

**Table 3. Cytotoxicity of 11j Against Wild Type (wt) and Notch-mutant (mut) Leukemia Cells**

| cell line | origin | Notch mutation | $GI_{50}$ (μM) (mean ± SE) |
|---|---|---|---|
| | resazurin assay | | |
| SUP-T11 | T-ALL[a] | wt | 2.20 ± 0.00 |
| LOUCY | T-ALL[a] | wt | 3.65 ± 0.05 |
| Jeco-1 | B-cell lymphoma | wt | >10 |
| Mino | B-cell lymphoma | wt | 5.7 ±0.9 |
| MOLT-16 | T-ALL[a] | wt | 7.4 ± 0.8 |
| HL-60 | promyelocytic leukemia | wt | >10 |
| Jurkat | T-ALL[a] | wt | 1.5 ± 0.3 |
| MOLT-4 | T-ALL[a] | mut | 0.14 ± 0.01 |
| HPB-ALL | T-ALL[a] | mut | 2.70 ± 0.06 |
| RPMI-8402 | T-ALL[a] | mut | >10 |
| Rec-1 | B-cell lymphoma | mut | 6.5 ± 0.2 |
| | NCI60 screen, SRB assay | | |
| HL-60 (TB) | acute myeloid leukemia | wt | 2.82 |
| K-562 | chronic myeloid leukemia | wt | 3.98 |
| CCRF-CEM | T-ALL[a] | mut | 1.47 |
| MOLT-4 | T-ALL[a] | mut | 0.0427 |

[a]T-ALL: T-cell acute lymphoblastic leukemia

We next attempted photoaffinity labeling to identify the molecular target(s) of BIPP **11**.[17] The key challenges to address when applying this approach included selection of a) a suitable linker and b) feasible attachment site to maintain biological activity of the resulting small molecule following photoactivation and covalent linking. In our study, nitrogen atom of the benzimidazole fragment (Scheme 2, $R_7$) and 4-OH group in the phenyl ring A (Scheme 1, $R_3$, **t** and **u)** were prioritized as potential connecting points, primarily due to the results from the SAR studies and relative ease of their chemical modification with photoreactive group. Compounds **11t** and **11u**, tentative analogues of **11j** containing *O*-alkyl groups, were synthesized from the corresponding aromatic aldehydes **2t** and **2u** (Scheme 1). Molecules **11bx**, **11by**, **11jx**, **11jy**, and **11jz**, substituted at the *N* atom of the benzamidazole fragment, were synthesized by alkylation of the corresponding precursors **11b** and **11j** with alkyl halides (Scheme 2). Unfortunately, we observed a considerable decrease in cytotoxicity of **11t**, **11jx**, and **11jy** against MOLT-4 cells (Table 2) even for the respective methyl derivative **11jx**. The sea urchin embryo tests further confirmed that modifications of the *N* atom in benzimidazole (**11bx**, **11by**, **11jx**, and **11jy**) or 4-hydroxy group of the A ring (**11t** and **11u**) with potential linker reduced or eliminated the activity of compounds (Table 1). A derivative of **11j** modified with the diazirine PAL linker,[18] **11jz**, (Scheme 2) didn't show any phenotypic effects in the sea urchin embryos (Table 1). In addition, modifications of the *N* atom of benzimidazole dramatically reduced solubility of the derivatives. We concluded that the positions selected for photoaffinity labeling were not suitable rendering the suggested photoaffinity labeling approach

unacceptable for target identification. In our assessment, a more in-depth search for the alternative linker attachment sites may require a significant investment into a rather involved and challenging chemistry. The next attempt for target identification included QSAR virtual screening model[19] *via* a free accessible website http://rfqsar.kaist.ac.kr/home.php. This model is based on the ChEMBL dataset of human proteins. The query results for **11j** including the top-10 from overall 1,288 potential targets are presented in Supplementary Figure S22. Kinases were found to be the most probable targets, FGFR1 leading the list (probability factor of 0.28 or 28%). Therefore, in the next series of experiments we evaluated the effect of **11j** on a panel of kinases (Supplementary Table S1). The panel comprised kinases associated with mitosis, apoptosis, different signaling pathways, including those participating in regulation of spiculogenesis. Unfortunately, the molecule did not display any notable inhibition of the receptor-type tyrosine-protein kinases (AURKA, FGFR2, FGFR4, FLT3, and ZAP70), non-receptor tyrosine-protein kinases (ABL1, ACVR1, BTK, JAK2, and Lyn), and serine/threonine-protein kinases (DAPK1, GSK3B, IRAK1, IRAK4, MAP3K7, MAP4K4, PRKCA, PRKCQ, STK4, STK17A, and STK17B) up to 10 μM concentration. Whereas it is still possible the molecule binds to other targets in the expanded kinome, we felt the selected panel was both sufficiently comprehensive and representative of all major kinase classes.

Next, we evaluated compounds **11j** and **12j** in a panel of matrix metalloproteinases (MMPs). The choice of MMPs was based on the ability of BIPP **11** to impair both hatching and spiculogenesis of the sea urchin embryos. The sea urchin embryos hatch from fertilization envelope at mid-blastula. At this stage, hatching enzyme (Zn-, Ca-dependent matrix metalloproteinase; envelyzin; EC 3.4.24.12)[20, 21] digests the fertilization envelope, and embryos start to swim. The majority of MOLT-4-selective BIPP **11** were found to be hatching suppressors, suggesting their possible interaction with MMPs. Literature data indicate that in addition to hatching regulation, MMPs in the sea urchin embryos participate in the primary mesenchyme cells (PMC) fusion and syncytium formation necessary for spiculogenesis,[22-24] as well as in the regulation of spicule elongation.[25] The target-based screen showed that **11j** did not exhibit any appreciable inhibitory activity against a set of MMPs, including MMP-1, 2, 8, 12, 13, 14, and ADAM17 (disintegrin and metalloproteinase domain-containing protein 17). Intriguingly, **11j** inhibited MMP-9 with the $IC_{50}$ value of *ca.* 490 nM, whereas **12j** used as a negative control was inactive. Considering the above results, we hypothesized that MMP-9 could be a molecular target. To verify the hypothesis, cytotoxicity of CGS 27023A (a reported inhibitor of MMP-1, MMP-2, MMP-3, and MMP-9[26]) was tested in the MOLT-4 cells to show no effect at concentrations up to 10 μM. Moreover, a tetracycline antibiotic doxycycline known to inhibit multiple MMP isoforms displayed average $GI_{50}$ value of 3.05 μM over 60 cell lines without any selectivity against MOLT-4 cells (NCI60 screen data, NSC # 756751; https://dtp.cancer.gov). For comparison, effects of four standard MMP inhibitors (GM6001, marimastat, CTS-1027, and T-5224) on the sea urchin embryos were assessed (Supplementary Table S2). In our hands, all tested MMP inhibitors failed to affect cleavage and/or embryo viability at concentrations up to 4 μM. Multiproteinase inhibitors GM6001 and marimastat both affected MMP-9, suppressed the embryo hatching at 0.02 μM and 0.05 μM,

respectively and inhibited spicule formation at 0.2 μM. Inhibitor of MMP-2 and MMP-13, CTS-1027, was less potent altering hatching and spiculogenesis at 1 μM and 4 μM concentrations, respectively. T-5224 reported to inhibit MMP-3 and MMP-13 was inactive. Interestingly, the most potent agents GM6001 and marimastat both reportedly target MMP-9 (https://www.medchemexpress.com), a MMP family member that was also inhibited by **11j**. However, in contrast to the reported MMP inhibitors, BIPP **11** altered spiculogenesis at markedly lower concentrations than those suppressing embryo hatching (Table 1), suggesting interaction with an additional molecular network(s) involved in the sea urchin embryo spicule formation. Considering these observations, MMP/MMP-9 could be one of the targets of BIPP **11**. However, this mode of action is not likely to be related to the selective inhibition of MOLT-4 cell growth.

Since all attempts of BIPP **11** target(s) identification summarized above were unsuccessful, in the next series of experiments we conducted a more detailed study focused on the specific impairment of spicule formation caused by BIPP. Spiculogenesis of the sea urchin embryo (Supplementary Figure S23) involves several steps including: 1) ingression of spiculogenic cells (PMCs, the only cells responsible for spicule formation and growth) at a blastula stage, approximately at 1–2 h post-hatching; 2) directional migration of PMC inside blastocoel by means of filopodia to afford two ventrolateral clusters during gastrulation; 3) PMC fusion to form a syncytium, and 4) spicule development, including uptake of $Ca^{2+}$ and $Mg^{2+}$ ions from seawater and secretion of skeletal material (carbonate Ca, less carbonate Mg, and spicule matrix proteins) into PMC syncytial cable *via* endocytosis.[27] Considering this evidence from the developmental biology, we selected a set of inhibitors that were likely to modulate signaling cascades and proteins involved in the spicule formation, and their effects were compared to the phenotypic changes caused by BIPP **11** (Figure 3, Supplementary Table S3). Specifically, we determined that when the control blastulas hatched from the fertilization envelope and started to swim (Figure 2B and Figure 3a), zygotes exposed to either BIPP (Figure 2B) or MMP inhibitors (Figure 3b) resulted in blastulas that continued to develop inside the fertilization envelope for several hours. At latter stages of development BIPP selectively inhibited spiculogenesis, but the embryos retained bilateral symmetry, normal motility and gut differentiation (Figure 2A).

Next, since mitogen-activated protein kinases (MAPK) were reported to play the key role in the sea urchin embryo skeletogenesis,[28-30] we tested several specific inhibitors of MAPKs (*ex.*, MEK1/2, ERK1/2, and Raf) (Supplementary Table S3). Multiple compounds caused selective concentration-dependent suppression of spicule formation up to complete spicule elimination when added to the fertilized eggs (Figure 3, panel e). However, as opposed to BIPP, they strongly inhibited ingression of the spiculogenic PMC at a blastula stage (Figure 3c, Supplementary Table S3) and caused exogastrulation with differentiated gut (Figure 3f, Supplementary Table S3) in accordance with the literature data. [28-30] Compounds that modulate transforming growth factor β/transforming growth factor β receptor (TGFβ/TGFβR) signaling pathway effectively suppressed spiculogenesis, however they also triggered radialization to produce a bell-shaped form embryos distinct from the species exposed to BIPP **11** (Figure

2A and Figure 3g,h, Supplementary Table S3). Similar effects of TGFβ/TGFβR inhibitors including SB431542 and RepSox on the sea urchin embryos from different species *Strongylocentrotus purpuratus* and *Lytechinus variegatus* have been reported.[31] PD173074, a potent inhibitor of both fibroblast growth factor receptor 1 (FGFR1) and vascular endothelial growth factor receptor 2 (VEGFR2) inhibited spicule growth at 1–4 μM concentration. However, the agent did not cause spicule elimination contrasting the observed BIPP effects (Supplementary Table S3). In addition, it was reported that the suppression of FGFR1 signaling by specific antisense morpholino oligonucleotides in the sea urchin embryos induced inhibition of skeletogenesis, gastrulation delay, prevented gut differentiation and pigment cells formation,[32] the effects not observed for BIPP. Likewise, perturbations in the VEGF/VEGFR signaling network led to the noticeable skeletal abnormalities along with the alteration of PMC migration.[33, 34]

Similarly to the cytotoxicity assessment on the wild type and Notch-mutant leukemia cell lines, the sea urchin embryo tests also confirmed Notch-independent mechanism of action of BIPP. Highly potent and selective Notch/γ-secretase inhibitors semagacestat and LY-411575 along with the Notch signaling inhibitor LY3039478 did alter spicule growth. However, as opposed to BIPP, they also induced a distinct inhibition of archenteron differentiation, secondary mesenchyme cells, coelomic pouches and pigment cells development (Figure 3i,j, Supplementary Table S3).

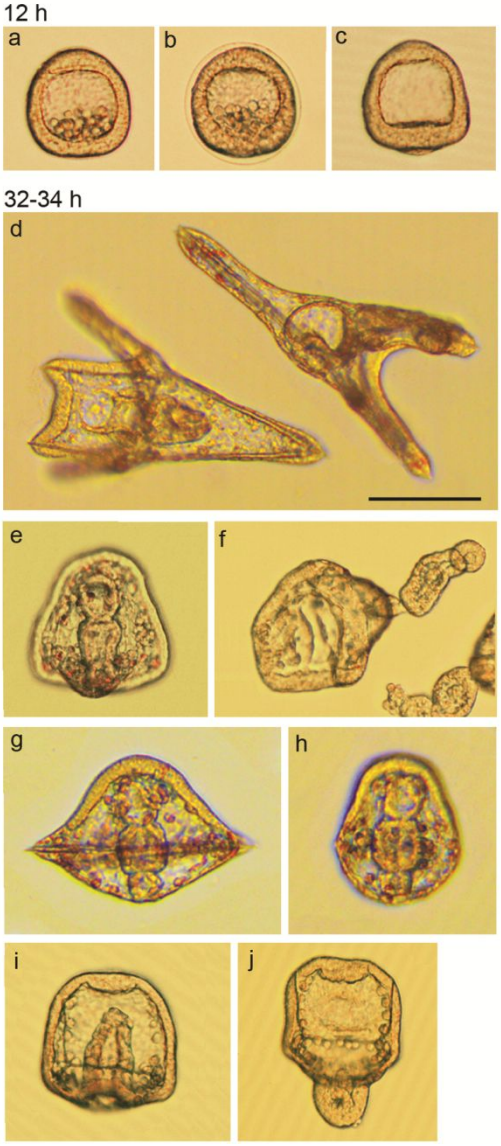


**Figure 3.** Developmental alterations of the sea urchin embryos in response to different inhibitors of spiculogenesis. (a) Intact mesenchyme blastula with primary mesenchyme cells (PMC) inside blastocoel. (b) Hatching arrest caused by matrix metalloproteinase inhibitor marimastat (2 μM). Mesenchyme blastula developed inside fertilization envelope. (c) PMC elimination after exposure of zygotes to MEK1/2 inhibitor trametinib (20 nM). (d) Control plutei with skeletal spicules and differentiated gut. (e) MEK1/2 inhibitor binimetinib (500 nM) produced embryos without spicules and caused exogastrulation (outward archenteron growth) with gut differentiation (f). (g) and (h) Bell-shaped radialized embryos exposed to TGFβR/Alk5 inhibitor RepSox at 0.2 μM (g) and 1 μM (h). (i) Suppression of archenteron (primary gut) and secondary mesenchyme cells formation by Notch inhibitor LY3039478 (1 μM). Some embryos exogastrulated (j). Short irregular spicules are present. (a)–(c) 12 h postfertilization. Average embryo diameter: 115 μm. (e)–(j): 32–34 h postfertilization. Bar: 100 μm. Incubation temperature: 24 °C.

Next, we probed other molecules for the selective cytotoxicity against MOLT-4 cells to identify murrayafoline A as a candidate. This natural product isolated from the root bark of *Murraya euchrestifolia* (Rutaceae) demonstrated potent selective cytotoxicity against MOLT-4 cells in NCI60 screen[35] with

MOLT-4 $GI_{50}$ = 0.025 μM (Supplementary Figure S24). It was found that murrayafoline A inhibited Wnt/β-catenin signaling by β-catenin degradation independent of GSK-3β, β-catenin phosphorylation and Siah-1/APC pathway.[36] This prompted us to test a hypothesis of potential targeting Wnt/β-catenin signaling cascade with BIPP. Specifically, we tested murrayafoline A as well as additional Wnt-modulating agents (IWR-1-endo, XAV-939, IWP-2, LGK-974, Wnt-C59, NCB-0846, and BML-284) in the sea urchin embryo model. The results are presented in Supplementary Table S3. Murrayafoline A caused cleavage alteration (EC = *ca* 1 μM) and cleavage arrest (EC = *ca* 8 μM), when applied to fertilized eggs. The arrested eggs acquired tuberculate shape typical of the effect caused by the microtubule destabilizing agents. The same outcome was observed for a very potent and specific Wnt/PORCN inhibitor, LGK-974, (EC = 1 and 4 μM for cleavage alteration and cleavage arrest, respectively). Whereas murrayafoline A and Wnt-targeting compounds inhibited spicule formation/growth, their phenotypic effect was different compared to that of BIPP (Supplementary Table S3), specifically, neither spiculogenesis nor hatching were affected significantly. Compound NCB-0846 was toxic resulting in the embryo mortality at concentrations ≥0.2 μM. Interestingly, known Wnt activator BML-284 caused cleavage alteration, cleavage arrest and embryo spinning at 0.01, 0.05, and 0.2 μM, respectively, evidencing strong antimitotic microtubule destabilizing activity reported earlier using tubulin polymerization assay.[37]

Considering the above, our results suggest that the molecular target(s) of BIPP **11** are unlikely to involve MEK1/2, TGFβ/TGFβR, FGFR, VEGF/VEGFR, Notch, and canonical Wnt/β-catenin signaling cascades. Furthermore, several additional molecular networks could be excluded from our evaluation. For example, whereas inhibition of phosphoinositide 3-kinase (PI3K) altered spicule growth, it also blocked embryo development at a gastrula stage.[38] Acetazolamide, an inhibitor of carbonic anhydrase that regulates biomineralization, suppressed spicule initiation and growth but also impeded PMC migration, prevented pigment cells formation and caused general developmental delay.[39] We did not observe these phenotypic changes with BIPP **11** series. To further confirm the results of our studies, an investigation of NCI cancer cell screen database (https://dtp.cancer.gov) for inhibitors of different signaling pathways did not reveal any MOLT-4 selective compounds. Specifically, as suggested by NCI screen database, inhibitors of MEK1/2 (cobimetinib, dabrafenib, sorafenib, and trametinib), VEGFR and FGFR (axitinib, cabozantinib, CH5183284, dovitinib, pazopanib, ponatinib, regorafenib, and sorafenib), epidermal growth factor receptor (EGFR) (afatinib, erlotinib, and lapatinib), PI3K (idelalisib, LY294002, and wortmannin), and Wnt/β-catenin signaling (berberine, calotropin, chromomycin $A_2$, nonactin, pyrvinium pamoate, and salinomycin) did not exhibit any selective cytotoxicity against MOLT-4 cells.

## CONCLUSIONS

In summary, 1,3-substituted pyrazolopyridinones **11–18** were synthesized using three-component domino reaction, and their biological effects were evaluated on the sea urchin embryo model. BIPP **11** caused a specific effect on the sea urchin embryos, namely inhibition of the embryo hatching and spiculogenesis.

These compounds exhibited unique selectivity against MOLT-4 cancer cell line in the human cancer cell screen. The sea urchin embryo test results indicated that BIPP cytotoxicity against MOLT-4 cells was unrelated to the antimitotic tubulin machinery. Detailed SAR examination of these compounds suggested that the observed MOLT-4 effect is likely a result of their interaction with the same cellular target(s) and/or molecular networks in both assay systems. This assumption is supported by the fact that numerous regulatory networks and signalling pathways common for other animals and humans were first described and investigated comprehensively in the sea urchin embryos.[40-43] Importantly, sea urchin and human genomes share more than 7,000 genes.[44] Subsequent studies of possible mechanisms that could mediate MOLT-4 specificity allowed us to eliminate Notch, Wnt/β-catenin, receptor tyrosine kinases (VEGF/VEGFR, FGF/FGFR), PI3K, and Raf-MEK-ERK signaling pathways as possible targets of BIPP. Although MMP-9/hatching enzyme was identified as one of the possible BIPP **11** targets, specific cytotoxicity against MOLT-4 cells was unrelated to this mode of action.

## EXPERIMENTAL PROCEDURES

**Chemistry.** *General Experimental Procedures.* Melting points were measured on a Boetius melting point apparatus and were uncorrected. $^{1}$H NMR and $^{13}$C NMR spectra were recorded on a Bruker DRX-500 instrument [working frequencies of 500.13 MHz ($^{1}$H) and 125.76 MHz ($^{13}$C)]. Chemical shifts were stated in parts per million (ppm) and referenced to the appropriate NMR solvent peaks. Spin-spin coupling constants (*J*) were reported in Hertz (Hz). NMR spectra (Supporting Information) were prepared using an original software designed at N. D. Zelinsky Institute of Organic Chemistry RAS (Moscow, Russian Federation) (http://nmr.ioc.ac.ru:8080/SDF2PDF.kl1). Low resolution mass spectra (*m*/*z*) were recorded on a Finnigan MAT/INCOS 50 mass spectrometer at 70 eV using direct probe injection. Elemental analysis was performed on the automated PerkinElmer 2400 CHN microanalyzer. Flash chromatography was carried out on silica gel (Acros, 0.035–0.070 mm, 60 Å). TLC was performed on Merck 60 $F_{254}$ plates. Solvents, Meldrum's acid, 3-iminobutanenitrile and benzaldehydes **2a**–**k** were purchased from Acros Organics (Belgium) at the highest commercial quality and used as received. Non-commercial benzaldehydes **2l**–**o**[45] and **2s**[14] were synthesized according to published procedures.

*Synthesis of 1-(1H-Benzimidazol-2-yl)-3-methyl-1H-pyrazol-5-amine (**3**).* A mixture of 2-hydrazinyl-1*H*-benzimidazole (**21**) (15.67g, 0.106 M) and 3-oxobutanenitrile (8.8 g, 0.106 M) in EtOH (100 mL) was heated for 40 min at 60–75 °C. The first precipitate was formed in 10 min. The reaction mixture was cooled (3 °C), the precipitate was filtered off, washed with cold EtOH (10 mL), ether (10 mL), and dried in air to afford **3** (12 g, 53% yield); mp 208–210 °C; $^{1}$H NMR (DMSO-$d_6$, 500 MHz): $\delta$ 2.16 (s, 3H, $CH_3$), 5.30 (s, 1H, H-4), 6.82 (s, 2H, $NH_2$), 7.15 (m, 2H, H-5',6'), 7.39 (m, 1H, H-4'), 7.53 (m, 1H, H-7'), 12.64 (s, 1H, NH); $^{13}$C NMR (DMSO-$d_6$, 125 MHz) $\delta$ 13.8, 87.7, 111.0, 117.5, 121.6, 121.7, 132.3, 141.6, 147.5, 149.5, 151.6. EIMS *m*/*z* 213 [M+] (100), 173 (26), 133 (21), 132 (19), 118 (27), 105 (15). Anal. Calcd for $C_{11}H_{11}N_5$: C, 61.96; H, 5.20; N, 32.84. Found: C, 61.83; H, 5.17; N, 32.92;

*General Procedure for the Three Component Condensation.* A mixture of 0.55 g (0.0038 mol) Meldrum's acid **1** in 7 mL of AcOH, aldehyde **2** (0.0033 mol), and aminopyrazole **3**–**10** (0.003 mol) was refluxed for 2 h. Then reaction mixture was concentrated *in vacuo* and the residue was triturated with 10 mL of EtOH. The resulting precipitate was filtered, washed with EtOH (3 × 7 mL) and dried to afford pure compounds **11**–**18**.

*General Procedure for Alkylation of 1-(Benzimidazol-2-yl)pyrazolo[3,4-b]pyridin-6-ones **11b** and **11j**.* A mixture of 1-(benzimidazol-2-yl)pyrazolo[3,4-b]pyridin-6-one **11b** or **11j** (1 mmol), alkylating agent (5 mmol MeI or 1.1 mmol *n*-$C_7H_{15}I$) and dried $K_2CO_3$ (1.1 mmol) in 3 mL of dry DMF was stirred at room temperature for 3 h and then diluted with water (10 mL). To prepare the respective *N*-methyl derivatives the resulting precipitate was filtered off, washed with water (2 mL) and EtOAc (2 mL) and dried. In order to access *N*-heptyl derivatives, the resulting suspension was extracted with EtOAc (2 × 5 mL), the combined extracts were evaporated to dryness and the residue was purified by column chromatography (heptane/EtOAc, 2:1). To synthesize the diaziridine derivative **11jz**, a mixture of **11j** (38 mg, 0.09 mmol), 3-(but-3-yn-1-yl)-3-(2-iodoethyl)-3*H*-diazirene (21 mg, 0.09 mmol) and dried $K_2CO_3$ (14 mg, 0.1 mmol) in 1 mL of dry DMF was stirred at 40–45 °C for 6 h and diluted with water (5 mL). The resulting suspension was extracted with EtOAc (2 × 5 mL), the combined extracts were concentrated *in vacuo* and the residue was purified by column chromatography (heptane/EtOAc, 2:1).

**Biology.** *Materials and Methods.* AS703026, AZ628, AZD8330, BML-284, cobimetinib, CTS-1027, dabrafenib, FR 180204, GDC-0623, GDC-0879, GDC-0994, GM6001, ITD-1, IWP-2, LY3039478, LY3200882, LY-411575, marimastat, NCB-0846, PD184352, PD318088, refametinib, RepSox, RO4987655, SB590885, SCH772984, selumetinib, semagacestat, T-5224, TAK-632, TAK-733, trametinib, ulixertinib, VX-11e, and Wnt-C59 were purchased from MedChem Express LLC, Monmouth Junction, NJ, USA. Binimetinib, EW-7197, GW788388, IWR-1-endo, LGK-974, PD173074, SB431542, and XAV-939 were purchased from Selleckchem, Houston, TX, USA. Murrayafoline A was purchased from Ark Pharm Inc., Arlington Heights, IL, USA. CGS 27023A was provided by Novartis. 3-(But-3-yn-1-yl)-3-(2-iodoethyl)-3*H*-diazirine was prepared as described previously.[18]

*Resazurin (Alamar Blue) Cytotoxicity Assay.*[15] The leukemia cell lines were obtained from the American Type Culture Collection (ATCC; HL-60, LOUCY, Mino, MOLT-4, MOLT-16, and Rec-1) and German Collection of Microorganisms and Cell Cultures GmbH (DSMZ; HPB-ALL, Jeco-1, Jurkat, RPMI-8402, and SUP-T11) and maintained in RPMI-1640 supplemented with 10–20% fetal bovine serum (Amimed #2-01F30-I)) and 2 mM L-glutamine (Supplementary Table S4). Cell lines were seeded at 40.000 cells per well in 100 µL of complete media in 96-well tissue-culture-treated microplates, flat bottom (TPP#92696). Compounds (10 mM in DMSO) were transferred to cells seeded in 96-well plates using HP dispenser to create a ten-point dose–response curve in triplicate starting from 1 uM with a 1:3 serial dilution. Cells were cultured in a humidified incubator set at 37 °C and maintained at an atmosphere of 5% $CO_2$. On Day 4, 10 µL per well of the resazurin reagent (Sigma #R7017 diluted in PBS as a stock

solution at 130 µg/mL, stored at 4 °C) was added. The plates were incubated at 37 °C for 4 h in an incubator after which fluorescence was read using a fluorescence plate reader at 560ex/590em, sensitivity 40 (Synergy HT from Biotek and Gen5 software). Normalized fluorescence intensity data were analyzed using XLfit, and subsequent $IC_{50}$ values were calculated using Dose Response one site 4 parameter logistic model.

*Biochemical Screen on Proteases.* All protein and peptide containing solutions were handled in siliconized tubes (Life Systems Design, Merenschwand, Switzerland). The compound solutions were transferred to 384-well assay plates (black Cliniplate; cat. no. 95040020 Labsystems Oy, Finland) by means of a CyBi-Hummingwell pipettor (CyBio AG, Jena, Germany). The enzyme and substrate solutions were transferred to the assay plates by means of a CyBi-well 384-channel pipettor (CyBio AG, Jena, Germany). For the determination of $IC_{50}$ values, the assays were performed at room temperature in 384-well plates with a total assay volume of 25.25 µL per well. The test compounds were dissolved in 90 % (v/v) DMSO/water. For the assays, 250 nL of the 90 % (v/v) DMSO/water solution or compound solution were added per well, followed by the addition of 12.5 µL protease solution (protease in buffer solution). The final assay concentrations of each enzyme are given in section Assay conditions. After 70 min of pre-incubation at room temperature, the reactions were started by the addition of 12.5 µL substrate solution (see section Assay conditions). After the addition of the substrate solution, the final DMSO concentration in the assay was 0.9 % (v/v). The effect of the compound on the enzymatic activity was obtained from the linear part of the progress curves and determined after 1 h (t = 60 min). The final compound concentrations ranged from 100 µM to 1 nM. Plate measurements were conducted with an Ultra reader (TECAN, Maennedorf, Switzerland). For fluorescence intensity (FI) measurements with the dye pairs EDANS/DABCYL and Mca/Dnp or the dye AMC, the instrument was equipped with a combination of a 350 nm (20 nm bandwidth) and a 500 nm (25 nm bandwidth) bandpass filter for fluorescence excitation and emission acquisition, respectively. For FI measurements with the dye Rh110, the instrument was equipped with a combination of a 485 nm (25 nm bandwidth) and a 535 nm (25 nm bandwidth) bandpass filter for fluorescence excitation and emission acquisition, respectively. To increase the signal:background ratio, appropriate dichroic mirrors were employed. All filters and dichroic mirrors were purchased from TECAN. The fluorophores in each well were excited by three flashes per measurement. The $IC_{50}$ values were calculated from the plot of percentage of inhibition vs. inhibitor concentration by a logistics fit according to

$$y = A2 + (A1 - A2) / (1 + (x/ IC50) \wedge p) \qquad \text{(Equation 1)}$$

where $y$ is the %-inhibition at the inhibitor concentration, $x$. A1 is the lowest inhibition value, i.e. 0 %, and A2 the maximum inhibition value, i.e. 100 %. The exponent, p, is the Hill coefficient. The curve fitting was conducted with the non-linear regression routine of the in-house software Helios.

Enzymes:

human MMP1 (Uniprot P03956) covering amino acids 1-469; expressed in and purified from stable transfected C127 cells

human MMP2 (Uniprot P08253) covering amino acids 1-660; expressed in and purified from insect cells (baculovirus expression system)

human MMP7 (Uniprot P09237) covering amino acids 95-267; expressed in and purified from *E.coli*

human MMP8 (Uniprot P22894) covering amino acids 100-262; expressed in and purified from *E.coli*

human MMP9 (Uniprot P14780) covering amino acids 1-707; expressed in and purified from stable transfected 293 cells

human MMP12 (Uniprot P39900) covering amino acids 101-268; expressed in and purified from *E.coli*

human MMP13 (Uniprot P45452) covering amino acids 103-274; expressed in and purified from *E.coli*

human MMP14 (Uniprot P50281) covering amino acids 112-284; expressed in and purified from *E.coli*

human TACE (Uniprot P78536) covering amino acids 1-670; expressed in and purified from insect cells (baculovirus expression system)

substrate: MCA-Pro-Leu-Gly-Leu-DPA-Ala-Arg-$NH_2$, purchased from Biosyntan (www.biosyntan.de), product number 6375

enzyme concentrations: 0.3 nM (MMP1), 8 nM (MMP2), 0.4 nM (MMP7), 1 nM (MMP8), 0.3 nM (MMP9), 1.5 nM (MMP12), 0.015 nM (MMP13), 0.2 nM (MMP14), 0.3 nM (TACE)

substrate concentration: 5 mM

assay buffer: 100 mM Tris, pH 7.4, 100 mM NaCl, 10 mM $CaCl_2$, 10 mM $ZnCl_2$, 0.075% (v/v) Brij35

*Phenotypic Sea Urchin Embryo Assay.*[13, 14] Adult sea urchins, *Paracentrotus lividus* (Echinidae), were collected from the Mediterranean Sea on the Cyprus coast and kept in an aerated seawater tank. Gametes were obtained by intracoelomic injection of 0.5 M KCl. Eggs were washed with filtered seawater and fertilized by adding drops of diluted sperm. Embryos were cultured at room temperature under gentle agitation with a motor-driven plastic paddle (60 rpm) in filtered seawater. The embryos were observed with a Biolam light microscope (LOMO, St. Petersburg, Russia). Microphotographs were obtained using an AmScope binocular microscope with an MU500 digital camera (United Scopes LLC, Irvine, CA, USA). For treatment with the test compounds, 5 mL aliquots of embryo suspension were transferred to six-well plates and incubated as a monolayer at a concentration up to 2000 embryos/mL. Stock solutions of tested molecules were prepared in DMSO at 10 mM concentration followed by a 10-fold dilution with 96% EtOH. This procedure enhanced the solubility of the test compounds in the salt-containing medium (seawater), as evidenced by microscopic examination of the samples. The maximal tolerated concentrations of DMSO and EtOH in the *in vivo* assay were determined to be 0.2% and 0.5%, respectively. Higher concentrations of either DMSO (≥0.5%) or EtOH (≥1%) caused nonspecific alteration and retardation of the sea urchin embryo development independent of the treatment stage. The antiproliferative activity was assessed by exposing fertilized eggs (8–15 min after fertilization, 45–55 min before the first mitotic cycle completion) to 2-fold decreasing concentrations of the compound. Cleavage

alteration and arrest were clearly detected at 2.5 h and 5.5 h after fertilization, when control embryos reached 8-cell and early blastula stages, respectively. The effects were estimated quantitatively as an effective threshold concentration, resulting in cleavage alteration and embryo death before hatching or full mitotic arrest. At these concentrations all tested microtubule destabilizers caused 100% cleavage alteration and embryo death before hatching, whereas at 2-fold lower concentrations the compounds failed to produce any effect. For microtubule-destabilizing activity, the compounds were tested on free-swimming blastulae just after hatching (8–10 h postfertilization), which originated from the same embryo culture. Embryo spinning was observed after 15 min to 20 h of treatment, depending on the structure and concentration of the compound. Both spinning and lack of forward movement were interpreted to be the result of the microtubule-destabilizing activity of a molecule. Video illustrations are available at http://www.chemblock.com. Sea urchin embryo assay data are available at http://www.zelinsky.ru. Experiments with the sea urchin embryos fulfill the requirements of biological ethics. The artificial spawning does not cause animal death, embryos develop outside the female organism, and both post spawned adult sea urchins and the excess of intact embryos are returned to the sea, their natural habitat.

## ASSOCIATED CONTENT

### Supporting Information

Analytical data for compounds **11**–**18**; NCI60 screen graphs for compounds **11a**, **11b**, **11f**, **11g**, **11i**, **11j**, **11k**, **11q**, **11r**, **16o**, and murrayafoline A; kinase screen and RF-QSAR data for compound **11j**; effects of inhibitors of spiculogenesis; leukemia cell lines description; schematic diagram of skeletogenic primary mesenchyme cells differentiation (Tables S1–S4, Figures S1–S24); $^{1}$H NMR spectra of compounds **11**–**18** (PDF)

## AUTHOR INFORMATION

### Corresponding Author

*Tel: +7 916 620 9584. Fax: +7 499 137 2966. E-mail: vs@zelinsky.ru.

### ORCID

Victor V. Semenov: 0000-0003-1889-341X

Alexei S. Karpov: 0000-0002-3067-4538

Alexander V. Samet: 0000-0002-0100-085X

Marina N. Semenova: 0000-0001-7656-9023

### Author Contributions

B.L., A.Kar., M.S., A.Kis. and V.S. conceived and designed the experiments, A.K., A.D., M.K., E.Kh., A.S., E.S., D.G., T.R., M.S. performed the experiments, A.Kar., L.K., M.S., A.Kis. and V.S. co-wrote the manuscript and Supporting Information. All authors have given approval to the final version of the

manuscript. We also wish to thank Dr. Yu. A. Strelenko from N. D. Zelinsky Institute of Organic Chemistry RAS for the development of NMR spectra presentation software.

**Funding**

The Russian Science Foundation, Grant 18-13-00044.

**Notes**

The authors declare no competing financial interest.

**ACKNOWLEDGMENTS**

We thank the National Cancer Institute (NCI) (Bethesda, MD, USA) for screening compounds by the Developmental Therapeutics Program at NCI (Anticancer Screening Program; http://dtp.cancer.gov). We wish to thank Academics Relations and Operational Alliances at Novartis for the general support. We are grateful to U. Hassiepen and Q. Zhiyan for their excellent technical assistance.

**Abbreviations:**

BIPP, benzimidazolyl-pyrazolo[3,4-*b*]pyridinone

EGFR, epidermal growth factor receptor

ERK, extracellular signal-regulated kinase

FGF/FGFR, fibroblast growth factor/fibroblast growth factor receptor

MAPK, mitogen-activated protein kinase

MMP, matrix metalloproteinase

PI3K, phosphoinositide 3-kinase

PMC, primary mesenchyme cells

SAR, structure-activity relationship

SRB, sulforhodamine B

T-ALL, T-cell acute lymphoblastic leukemia

TGFβ/TGFβR, transforming growth factor β/transforming growth factor β receptor

VEGF/VEGFR, vascular endothelial growth factor/vascular endothelial growth factor receptor

**Table of Content Graphic**

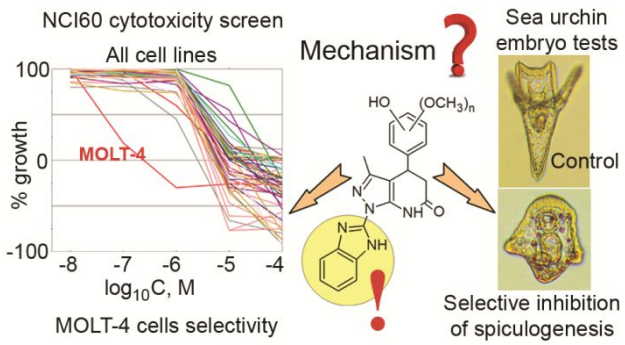

**References**

1. Lichitsky, B. V.; Komogortsev, A. N.; Belyi, R. M.; Dudinov, A. A.; Krayushkin, M. M. Three-Component Condensation of 4-Aminoisothiazole Derivatives with Aldehydes and Meldrum's Acid. Synthesis of 6,7-Dihydro-4H-Isothiazolo[4,5-b]Pyridin-5-Ones. *Russ. Chem. Bull.* **2009**, *58*, 1538–1541.

2. Semenov, V. V.; Lichitsky, B. V.; Komogortsev, A. N.; Dudinov, A. A.; Krayushkin, M. M.; Konyushkin, L. D.; Atamanenko, O. P.; Karmanova, I. B.; Strelenko, Y. A.; Shor, B.; Semenova, M. N.; Kiselyov, A. S. Synthesis and Anti-Mitotic Activity of 6,7-Dihydro-4H-Isothiazolo[4,5-B]Pyridin-5-Ones: In Vivo and Cell-Based Studies. *Eur. J. Med. Chem.* **2017**, *125*, 573–585.

3. Azimi Roshan, A.; Mamaghani, M.; Mahmoodi, N. O.; Shirini, F. Cheminform Abstract: An Efficient Regioselective Sonochemical Synthesis of Novel 4-Aryl-3-Methyl-4,5-Dihydro-1H-Pyrazolo[3,4-b]Pyridin-6(7H)-Ones. *Chin. Chem. Lett.* **2012**, *23*, 399–402.

4. Mamaghani, M.; Shirini, F.; Mahmoodi, N. O.; Azimi-Roshan, A.; Hashemlou, H. A Green, Efficient and Recyclable Fe+3@K10 Catalyst for the Synthesis of Bioactive Pyrazolo[3,4-b]Pyridin-6(7H)-Ones under "on Water" Conditions. *J. Mol. Struct.* **2013**, *1051*, 169–176.

5. Zhong, X.; Dou, G.; Wang, D. Polyethylene Glycol (PEG-400): An Efficient and Recyclable Reaction Medium for the Synthesis of Pyrazolo[3,4-b]Pyridin-6(7H)-One Derivatives. *Molecules* **2013**, *18*, 13139–13147.

6. Veisi, H.; Maleki, A.; Jahangard, S. Electrogenerated Base Promoted Synthesis of 3-Methyl-4-Aryl-2,4,5,7-Tetrahydropyrazolo[3,4-b]Pyridin-6-Ones Via Multicomponent Reactions of 5-Methylpyrazol-3-Amine, Aldehydes, and Meldrum's Acid. *Tetrahedron Lett.* **2015**, *56*, 1882–1886.

7. Hemmati, S.; Safarimehr, P.; Safaei, M.; Hekmati, M. One-Pot Green Synthesis of 3-Methyl-4-Aryl-2,4,5,7-Tetrahydropyrazolo[3,4-b]Pyridine-6-Ones by Multicomponent Assembling of 5-Methylpyrazol-3-Amine, Aldehydes, and Meldrum's Acid Using Sodium Dodecyl Sulfate (SDS) in Water. *J. Heterocyclic Chem.* **2017**, *54*, 1640–1644.

8. Sindhu, J.; Singh, H.; Khurana, J. M.; Bhardwaj, J. K.; Saraf, P.; Sharma, C. Synthesis and Biological Evaluation of Some Functionalized 1H-1,2,3-Triazole Tethered Pyrazolo[3,4-b]Pyridin-6(7H)-Ones as Antimicrobial and Apoptosis Inducing Agents. *Med. Chem. Res.* **2016**, *25*, 1813–1830.

9. Zeng, L.-Y.; Liu, T.; Yang, J.; Yang, Y.; Cai, C.; Liu, S. "On-Water" Facile Synthesis of Novel Pyrazolo[3,4-b]Pyridinones Possessing Anti-Influenza Virus Activity. *ACS Comb. Sci.* **2017**, *19*, 437–446.

10. Pettus, L. H.; Tasker, A.; Xu, S.; Wurz, R. Pyrazolo-Pyridinone Derivatives and Methods of Use. Patent WO/2009/055033, 2009.

11. Wager, T. T. Pyrazolo[3,4-b]Pyridin-6-Ones as Gsk-3 Inhibitors. Patent WO2005000303A1, 2005.

12. Frimurer, T. M.; Mende, F.; Graae, A.-S.; Engelstoft, M. S.; Egerod, K. L.; Nygaard, R.; Gerlach, L.-O.; Hansen, J. B.; Schwartz, T. W.; Holst, B. Model-Based Discovery of Synthetic Agonists for the Zn2+-Sensing G-Protein-Coupled Receptor 39 (GPR39) Reveals Novel Biological Functions. *J. Med. Chem.* **2017**, *60*, 886–898.

13. Semenova, M. N.; Kiselyov, A.; Semenov, V. V. Sea Urchin Embryo as a Model Organism for the Rapid Functional Screening of Tubulin Modulators. *BioTechniques* **2006**, *40*, 765–774.

14. Semenova, M. N.; Demchuk, D. V.; Tsyganov, D. V.; Chernysheva, N. B.; Samet, A. V.; Silyanova, E. A.; Kislyi, V. P.; Maksimenko, A. S.; Varakutin, A. E.; Konyushkin, L. D.; Raihstat, M. M.; Kiselyov, A. S.; Semenov, V. V. Sea Urchin Embryo Model as a Reliable in Vivo Phenotypic Screen to Characterize Selective Antimitotic Molecules. Comparative Evaluation of Combretapyrazoles, -Isoxazoles, -1,2,3-Triazoles, and -Pyrroles as Tubulin-Binding Agents. *ACS Comb. Sci.* **2018**, *20*, 700–721.

15. Riss, T. L.; Moravec, R. A.; Niles, A. L.; Duellman, S.; Benink, H. A.; Worzella, T. J.; Minor, L., Cell Viability Assays. In *Assay Guidance Manual [Internet]*, Sittampalam, G. S.; Coussens, N. P.; Brimacombe, K.; et al., Eds. Eli Lilly & Company and the National Center for Advancing Translational Sciences; 2004. Bethesda (MD), USA, 2013.

16. Walzl, A.; Unger, C.; Kramer, N.; Unterleuthner, D.; Scherzer, M.; Hengstschlager, M.; Schwanzer-Pfeiffer, D.; Dolznig, H. The Resazurin Reduction Assay Can Distinguish Cytotoxic from Cytostatic Compounds in Spheroid Screening Assays. *J. Biomol. Screen.* **2014**, *19*, 1047–1059.

17. Smith, E.; Collins, I. Photoaffinity Labeling in Target- and Binding-Site Identification. *Future Med. Chem.* **2015**, *7*, 159–183.

18. Li, Z.; Hao, P.; Li, L.; Tan, C. Y. J.; Cheng, X.; Chen, G. Y. J.; Sze, S. K.; Shen, H.-M.; Yao, S. Q. Design and Synthesis of Minimalist Terminal Alkyne-Containing Diazirine Photo-Crosslinkers and Their Incorporation into Kinase Inhibitors for Cell- and Tissue-Based Proteome Profiling. *Angew. Chem. Int. Ed.* **2013**, *52*, 8551–8556.

19. Lee, K.; Lee, M.; Kim, D. Utilizing Random Forest QSAR Models with Optimized Parameters for Target Identification and Its Application to Target-Fishing Server. *BMC Bioinformatics* **2017**, *18, Suppl.16*, 567.

20. Roe, J. L.; Lennarz, W. J. Biosynthesis and Secretion of the Hatching Enzyme During Sea Urchin Embryogenesis. *J. Biol. Chem.* **1990**, *265*, 8704–8711.

21. Gache, C.; Lepage, T.; Croce, J.; Lhomond, G. 151. Envelysin. In *Handbook of Proteolytic Enzymes*, 2nd ed.; Barrett, A. J.; Woessner, J.; Rawlings, N., Eds. Elsevier Academic Press: London, UK; San-Diego, California, USA, 2004; Vol. 1, pp 575–578.

22. Roe, J. L.; Park, H. R.; Strittmatter, W. J.; Lennarz, W. J. Inhibitors of Metalloendoproteases Block Spiculogenesis in Sea Urchin Primary Mesenchyme Cells. *Exp. Cell Res.* **1989**, *181*, 542–550.

23. Lennarz, W. J.; Strittmatter, W. J. Cellular Functions of Metallo-Endoproteinases. *BBA-Rev. Biomembranes* **1991**, *1071*, 149–158.

24. Ikegami, S.; Kobayashi, H.; Myotoishi, Y.; Ohta, S.; Kato, K. H. Selective Inhibition of Exoplasmic Membrane Fusion in Echinoderm Gametes with Jaspisin, a Novel Antihatching Substance Isolated from a Marine Sponge. *J. Biol. Chem.* **1994**, *269*, 23262–23267.

25. Ingersoll, E. P.; Wilt, F. H. Matrix Metalloproteinase Inhibitors Disrupt Spicule Formation by Primary Mesenchyme Cells in the Sea Urchin Embryo. *Dev. Biol.* **1998**, *196*, 95–106.

26. MacPherson, L. J.; Bayburt, E. K.; Capparelli, M. P.; Carroll, B. J.; Goldstein, R.; Justice, M. R.; Zhu, L.; Hu, S.; Melton, R. A.; Fryer, L.; Goldberg, R. L.; Doughty, J. R.; Spirito, S.; Blancuzzi, V.; Wilson, D.; O'Byrne, E. M.; Ganu, V.; Parker, D. T. Discovery of CGS 27023A, a Non-Peptidic, Potent, and Orally Active Stromelysin Inhibitor That Blocks Cartilage Degradation in Rabbits. *J. Med. Chem.* **1997**, *40*, 2525–2532.

27. Killian, C. E.; Wilt, F. H. Endocytosis in Primary Mesenchyme Cells During Sea Urchin Larval Skeletogenesis. *Exp. Cell Res.* **2017**, *359*, 205–214.

28. Kumano, M.; Foltz, K. R. Inhibition of Mitogen Activated Protein Kinase Signaling Affects Gastrulation and Spiculogenesis in the Sea Urchin Embryo. *Dev. Growth Differ.* **2003**, *45*, 527–542.

29. Fernandez-Serra, M.; Consales, C.; Livigni, A.; Arnone, M. I. Role of the ERK-Mediated Signaling Pathway in Mesenchyme Formation and Differentiation in the Sea Urchin Embryo. *Dev. Biol.* **2004**, *268*, 384–402.

30. Rottinger, E.; Besnardeau, L.; Lepage, T. A Raf/MEK/ERK Signaling Pathway Is Required for Development of the Sea Urchin Embryo Micromere Lineage through Phosphorylation of the Transcription Factor Ets. *Development* **2004**, *131*, 1075–1087.

31. Sun, Z.; Ettensohn, C. A. TGF-beta Sensu Stricto Signaling Regulates Skeletal Morphogenesis in the Sea Urchin Embryo. *Dev. Biol.* **2017**, *421*, 149–160.

32. Rottinger, E.; Saudemont, A.; Duboc, V.; Besnardeau, L.; McClay, D.; Lepage, T. FGF Signals Guide Migration of Mesenchymal Cells, Control Skeletal Morphogenesis [Corrected] and Regulate Gastrulation During Sea Urchin Development. *Development* **2008**, *135*, 353–365.

33. Duloquin, L.; Lhomond, G.; Gache, C. Localized VEGF Signaling from Ectoderm to Mesenchyme Cells Controls Morphogenesis of the Sea Urchin Embryo Skeleton. *Development* **2007**, *134*, 2293–2302.

34. Adomako-Ankomah, A.; Ettensohn, C. A. Growth Factor-Mediated Mesodermal Cell Guidance and Skeletogenesis During Sea Urchin Gastrulation. *Development* **2013**, *140*, 4214–4225.

35. Itoigawa, M.; Kashiwada, Y.; Ito, C.; Furukawa, H.; Tachibana, Y.; Bastow, K. F.; Lee, K. H. Antitumor Agents. 203. Carbazole Alkaloid Murrayaquinone A and Related Synthetic Carbazolequinones as Cytotoxic Agents. *J. Nat. Prod.* **2000**, *63*, 893–897.

36. Choi, H.; Gwak, J.; Cho, M.; Ryu, M. J.; Lee, J. H.; Kim, S. K.; Kim, Y. H.; Lee, G. W.; Yun, M. Y.; Cuong, N. M.; Shin, J. G.; Song, G. Y.; Oh, S. Murrayafoline A Attenuates the Wnt/beta-Catenin Pathway by Promoting the Degradation of Intracellular Beta-Catenin Proteins. *Biochem. Biophys. Res. Commun.* **2010**, *391*, 915–920.

37. Fukuda, Y.; Sano, O.; Kazetani, K.; Yamamoto, K.; Iwata, H.; Matsui, J. Tubulin Is a Molecular Target of the Wnt-Activating Chemical Probe. *BMC Biochem.* **2016**, *17*, 9.

38. Bradham, C. A.; Miranda, E. L.; McClay, D. R. PI3K Inhibitors Block Skeletogenesis but Not Patterning in Sea Urchin Embryos. *Dev. Dynam.* **2004**, *229*, 713–721.

39. Zito, F.; Koop, D.; Byrne, M.; Matranga, V. Carbonic Anhydrase Inhibition Blocks Skeletogenesis and Echinochrome Production in Paracentrotus Lividus and Heliocidaris Tuberculata Embryos and Larvae. *Dev. Growth Differ.* **2015**, *57*, 507–514.

40. Pederson, T. The Sea Urchin's Siren. *Dev. Biol.* **2006**, *300*, 9-14.

41. McClay, D. R. Evolutionary Crossroads in Developmental Biology: Sea Urchins. *Development* **2011**, *138*, 2639–2648.

42. Ernst, S. G. Offerings from an Urchin. *Dev. Biol.* **2011**, *358*, 285–294.

43. Range, R. C.; Martinez-Bartolome, M.; Burr, S. D. The Power of Simplicity: Sea Urchin Embryos as in Vivo Developmental Models for Studying Complex Cell-to-Cell Signaling Network Interactions. *J. Visualized Exp.* **2017**, e55113.

44. Di Bernardo, M.; Di Carlo, M. The Sea Urchin Embryo: A Model for Studying Molecular Mechanisms Involved in Human Diseases and for Testing Bioactive Compounds. In *Sea Urchin - from Environment to Aquaculture and Biomedicine*, Agnello, M., Ed. InTech: Rijeka, Croatia, 2017; pp 119–144.

45. Semenov, V. V.; Kiselyov, A. S.; Titov, I. Y.; Sagamanova, I. K.; Ikizalp, N. N.; Chernysheva, N. B.; Tsyganov, D. V.; Konyushkin, L. D.; Firgang, S. I.; Semenov, R. V.; Karmanova, I. B.; Raihstat, M. M.; Semenova, M. N. Synthesis of Antimitotic Polyalkoxyphenyl Derivatives of Combretastatin Using Plant Allylpolyalkoxybenzenes. *J. Nat. Prod.* **2010**, *73*, 1796–1802.